Journal of Advanced Ceramics
2013, 2(2): 173–179
DOI: 10.1007/s40145-013-0058-9 ISSN 2226-4108

Research Article

Synthesis of $Mg(OH)_2$ micro/nano flowers at room temperature

Pradip Sekhar DAS[a], Arjun DEY[b], Ashok Kumar MANDAL[a], Nitai DEY[a], Anoop K. MUKHOPADHYAY[a,*]

[a]*CSIR-Central Glass and Ceramic Research Institute*, *Kolkata 700032*, *India*
[b]*Thermal Systems Group*, *ISRO Satellite Centre*, *Vimanapura Post*, *Bangalore 560017*, *India*

Received: January 08, 2013; Revised: March 22, 2013; Accepted: March 24, 2013

Abstract: The inexpensive and green method of synthesis for self-assembled micro/nano structures is an important area of emerging research. Such structures can be chemically tuned with predesigned functional properties. Therefore, they hold very good promise for future applications, e.g., biomedicine, electronic device, solar energy, gas sensing. Here we report for the first time an inexpensive and green method for chemical deposition of magnesium hydroxide ($Mg(OH)_2$) micro/nano flowers in thin films on commercial soda lime silica glass substrates at room temperature. Under identical conditions, chemically synthesized $Mg(OH)_2$ powders are also prepared in absence of the soda lime silica glass substrates. The condition that favors the growth of micro/nano flowers in thin films is identified from X-ray diffraction (XRD), scanning electron microscopy (SEM), field emission scanning electron microscopy (FE-SEM), transmission electron microscopy (TEM), and energy dispersive X-ray spectroscopy (EDX) data. Finally, the possible growth mechanism of micro/nano flowers in thin films is discussed.

Keywords: magnesium hydroxide ($Mg(OH)_2$); flower-like microstructure; chemical deposition; film

1 Introduction

The thin films of self-assembled micro/nano-structured layered double hydroxides promise a very important area of emerging research [1–6]. Such research efforts are of crucial significance for a wide variety of promising applications, e.g., biological micro-reactors [1], targeted drug delivery [2], advanced catalysis [3], optoelectronic devices [4], buffer layers for thin film, and dye-sensitized solar cells [5,6]. In such approaches, metals like magnesium, nickel, zinc and copper, have been utilized to obtain the thin films of self-assembled micro/nano-structured layered double hydroxides.

* Corresponding author.
E-mail: anoopmukherjee@cgcri.res.in,
mukhopadhyay.anoop@gmail.com

There are many methods reported in the literature for the synthesis of magnesium hydroxide ($Mg(OH)_2$) powders. The typical techniques are, for instance, electrochemical deposition [7,8], hydrothermal synthesis [9] and precipitation [10]. The surfactant-mediated solution route [11] also has been utilized to obtain $Mg(OH)_2$ powders. On the other hand, the growth of ultra-thin $Mg(OH)_2$ films could only be realized by a high-temperature dynamic in-situ growth process [12]. Mostly, in the cases of powders, the formations of $Mg(OH)_2$ nano flakes [13], nano tubes [14], nano rods [15–17] and nano flowers [18,19] have been reported.

The more conventional usage of $Mg(OH)_2$ as powders or in thin film form is a thermally stable and environment friendly flame retardant [14,16]. The reason for such usage on a relatively much larger

commercial scale lies in the fact that $Mg(OH)_2$ is a both non-toxic and non-corrosive material [14,16]. In addition, $Mg(OH)_2$ is also utilized as a neutralizer in the treatment of acidic waste [17].

On the other hand, the more advanced applications require, e.g., porous $Mg(OH)_2$/MgO micro/nano flowers which can offer a very significant increase in adsorption sites due to the very presence of the hierarchical micro/nano structure. Such hierarchical architecture of the micro/nano structure allows the detection of both Pb(II) and Cd(II) ions [19]. It is already well known that both of these ions are highly toxic in nature and hence dangerous for the environment [19].

Further, these nano flowers are often utilized as large-band-gap (e.g., 5.17 eV) semi-conducting materials in the next-generation solar cells [5,6]. Nevertheless, it is almost needless to say that all the aforesaid methods [7–11] are not only cost intensive but also energy intensive. This information establishes the bare fact that there is a huge scientific and technological need to develop an inexpensive and green chemical deposition technique for $Mg(OH)_2$ micro/nano flower structures in both powder and thin film forms.

However, to the best of our knowledge, there is no study reported yet on the inexpensive and green chemical deposition technique for $Mg(OH)_2$ micro/nano flower structures in thin films at room temperature. Therefore, the objective of the present work is to develop $Mg(OH)_2$ thin films with a micro/nano flower structure on commercially available soda lime silica (SLS) glass substrates. The idea behind the choice of the commercial SLS glass as substrate is simply that, if the deposition technique becomes successful, the cost of substrates for advanced applications such as a detector for Pb(II) and Cd(II) ions [19], can still be kept on the lower side.

2 Materials and methods

$Mg(OH)_2$ thin films were deposited onto pre-cleaned and dried commercially available SLS glass slides (25 mm × 25 mm × 1.15 mm) by alternate dipping for requisite number of times at room temperature (30 ℃). The precursor solutions utilized for this purpose were 0.1 molar aqueous solutions of $Mg(NO_3)_2$ (analytical reagent grade, Ranbaxy, Mumbai, India) and NaOH (analytical reagent grade, Qualigens Fine Chemicals, Kolkata, India). The details of the synthesis process for $Mg(OH)_2$ thin films on SLS glass substrates have been already described by us elsewhere [20,21] and hence will not be repeated here for the sake of brevity.

In short, the number of dipping times was typically varied in the range from 2 to 60. The change in the mass of $Mg(OH)_2$ thin films obtained by the dip coating method was measured in a conventional chemical balance (Model No. AE163, Mettler, USA) that had a resolution of 10^{-4} g. Thus the data about the mass of the chemically deposited $Mg(OH)_2$ thin films could be obtained as a function of the number of dipping times.

Further, to check out what happened if the substrate was deliberately made absent, the $Mg(OH)_2$ powders were also synthesized keeping the same molar ratio of the reactants as used for the deposition of $Mg(OH)_2$ thin films. In addition, BET (Brunauer–Emmett–Teller) surface area measurement was performed by N_2 gas adsorption method (Twin Surface Area Analyzer, Quantachrome Instruments, USA).

Phase analysis of both the powders and thin films of $Mg(OH)_2$ synthesized in the present work were investigated by X-ray diffraction (XRD) technique in a standard diffractometer (PANalytical X'pert Pro MPD Diffractometer, the Netherlands). Microstructure characterizations of $Mg(OH)_2$ powders and thin films were carried out utilizing scanning electron microscopy (SEM, Model s430i, Leo, UK), field emission scanning electron microscopy (FE-SEM, Model Supra VP35, Carl Zeiss, Germany), transmission electron microscopy (TEM, Model Tecnai G^2 30, S-Twin, 300 KV, FEI, the Netherlands), and energy dispersive X-ray spectroscopy (EDX) data obtained during TEM work.

3 Results and discussion

The data about the change in the mass of $Mg(OH)_2$ thin films obtained by the dip coating method as a function of the total number of dipping times are summarized in Table 1. It may be seen easily that the rate of change of mass with the number of dipping times is not linear. For instance, between the 2nd dipping and the 20th dipping, the rate of change of mass per unit area of $Mg(OH)_2$ thin films is 0.225 μmol/cm^2 per dipping. However, between the 20th dipping and the 30th dipping, the rate of change of mass per unit area of $Mg(OH)_2$ thin films is steeply

hiked about 2.6 times to 0.585 μmol/cm^2 per dipping. As the number of dipping times is further enhanced from 30 to 60, the rate of change of mass per unit area of $Mg(OH)_2$ thin films settles out sluggishly to a little lower value of 0.161 μmol/cm^2 per dipping.

Table 1 The change of mass per unit area of the chemically deposited $Mg(OH)_2$ thin films on SLS glass substrates as a function of number of dipping times

Number of dipping	Mass (μmol/cm^2)
2	0.45±0.1
20	4.50±0.2
30	10.35±0.9
60	15.20±0.3

These data strongly suggest that around such higher number of dipping times, e.g., 60 times of dipping, the film deposition process is almost close to a point of saturation. Thus, it is established beyond doubt that the maximum rate of change of mass per unit area of $Mg(OH)_2$ thin films per dipping is attained between the 20th dipping and the 30th dipping. These data also suggest that some unique changes are most likely to occur in the film microstructure just below or at the 30th dipping and beyond the 30th dipping. This point shall be illustrated further later in terms of the electron microscopic evidences.

The representative XRD data of the chemically deposited $Mg(OH)_2$ thin films are shown in Fig. 1(a), while the similar data for $Mg(OH)_2$ powders are shown in Fig. 1(b). The data presented in Fig. 1(a) show peaks corresponding to the (001), (100), (101), (102), (110),

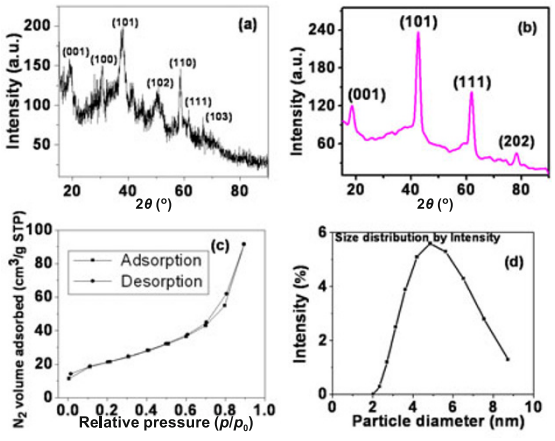

Fig. 1 XRD patterns of (a) $Mg(OH)_2$ thin films chemically deposited on SLS glass and (b) chemically synthesized $Mg(OH)_2$ powders; (c) specific surface area and (d) particle size distribution of the chemically synthesized $Mg(OH)_2$ powders.

(111) and (103) planes for the chemically deposited $Mg(OH)_2$ thin films. These peaks are the most characteristic peaks of phase-pure $Mg(OH)_2$ according to the data available for the standard material from JCPDS 7-239. Further, the d values for the respective inter planar spacing are calculated from the XRD peaks for (001), (100), (101), (102), (110), (111) and (103) planes. These d values are 4.7 Å, 2.9 Å, 2.4 Å, 1.8 Å, 1.6 Å, 1.5 Å and 1.4 Å, respectively. Thus, the data obtained on d values in the present work are in good agreement with the data reported for the standard material from JCPDS 7-239.

On the other hand, XRD data of the powders (Fig. 1(b)) show the presence of only four characteristic peaks, i.e., those from the planes (001), (101), (111) and (202). The corresponding d values are 4.8 Å, 2.15 Å, 1.5 Å and 1.22 Å, respectively. The d values measured from the experimental data are comparable to those standard data from JCPDS 7-239. However, for the same set of planes, the peaks measured for $Mg(OH)_2$ powders chemically deposited in absence of SLS glass substrates have intensities much higher than those obtained in the case of $Mg(OH)_2$ thin films on SLS glass substrates.

The corresponding lattice constants for $Mg(OH)_2$ thin films are calculated following the standard method described in Ref. [18]. The values are $a = b = 3.15$ Å and $c = 4.79$ Å. These data also match very closely with those (e.g., $a = b = 3.15$ Å and $c = 4.78$ Å) reported by other researchers in Ref. [18].

In the case of the chemically synthesized $Mg(OH)_2$ powders in absence of SLS glass substrates, the values of lattice constants are $a = b = 2.79$ Å and $c = 4.80$ Å. Thus, it would appear that for the chemically synthesized $Mg(OH)_2$ powders, the lattice constants along the mutually perpendicular crystallographic directions a and b are slightly smaller in comparison with the values in the same two directions of the corresponding thin films.

In spite of the fact that $Mg(OH)_2$ thin films synthesized in the present work are almost phase pure, it must be recognized that there are two unidentified peaks at $2\theta = 40°$–$50°$ in the current XRD data (Fig. 1(a)). Recently, similar observations are also reported by Lv *et al*. [22]. However, the intensities of these two unidentified peaks are insignificant in comparison with those main characteristic peaks from the (101) and (102) planes. It is suggested that these peaks possibly have arisen from the minor presence of the precursor materials, e.g., magnesium nitrate [23]. It is interesting

to note that no such unidentified peaks are present in the XRD data of the chemically synthesized $Mg(OH)_2$ powders (Fig. 1(b)).

In addition, the crystallite sizes of $Mg(OH)_2$ thin films are estimated corresponding to the broadened peaks (001), (100), (101), (102), (110), (111) and (103), respectively. The well-known Scherrer's method is employed to obtain these data [24]. However, before the application of Scherrer's method to the present XRD data, the data are corrected for the machine back-ground effect. The estimated crystallite sizes are about 1.8 nm, 4.8 nm, 3.7 nm, 9.3 nm, 6.0 nm, 2.9 nm and 5.6 nm for the broadened peaks obtained in the XRD data corresponding to the (001), (100), (101), (102), (110), (111) and (103) planes of $Mg(OH)_2$ thin films, respectively. Thus, the average crystallite size is estimated to be about 4.8±2.3 nm, which possibly reflects a heterogeneous distribution of the estimated crystallite sizes in $Mg(OH)_2$ thin films as expected.

However, in the case of the chemically synthesized powders, the estimated crystallite sizes are about 4.5 nm, 5.2 nm, 5.1 nm and 4.62 nm respectively for the peaks corresponding to the (001), (101), (111) and (202) planes. Thus, the average crystallite size is 4.9±0.4 nm. A comparison of the data for the chemically synthesized $Mg(OH)_2$ powders in absence of SLS glass substrates with those of $Mg(OH)_2$ thin films chemically deposited on SLS glass substrates would clearly suggest that the average values of the crystallite size are similar in both cases. But the major point of importance that arises out of this exercise is the fact that the uniformity of the crystallite size distribution in the chemically synthesized $Mg(OH)_2$ powders is much better than that of the chemically deposited $Mg(OH)_2$ thin films.

The data on the specific surface area of the chemically synthesized $Mg(OH)_2$ powders in absence of SLS glass substrates are shown in Fig. 1(c). The surface area is measured as 92.22 m²/g. Thus, the present data is much higher than the data reported [25,26] for micron-sized $Mg(OH)_2$ powders. It is quite obvious that the higher the specific surface area is, the smaller the average particle size will be. In fact, for the chemically synthesized $Mg(OH)_2$ powders, the particle size distribution data (Fig. 1(d)) show an average size of 4.7±2.2 nm. It is interesting to note that for the chemically synthesized $Mg(OH)_2$ powders, the average particle size data of 4.7±2.2 nm matches favourably with the average crystallite size of 4.9±0.4 nm.

The data on the development of microstructure as a function of the number of dipping times for the chemically deposited $Mg(OH)_2$ thin films are shown in Figs. 2(a)–2(d). Initially, just after two dippings, the film has a porous microstructure (Fig. 2(a)). Slowly, with the increase in the number of dipping times, e.g., after 20 dippings, the microstructure grows into a layered structure (Fig. 2(b)).

After 30 dippings, the microstructure of the chemically deposited $Mg(OH)_2$ thin films has changed into the architecture of unique porous micro/nano flowers (Fig. 2(c)). However, this unique porous micro/nano flower microstructure has disappeared at higher number of dipping times, e.g., 60 dippings (Fig. 2(d)).

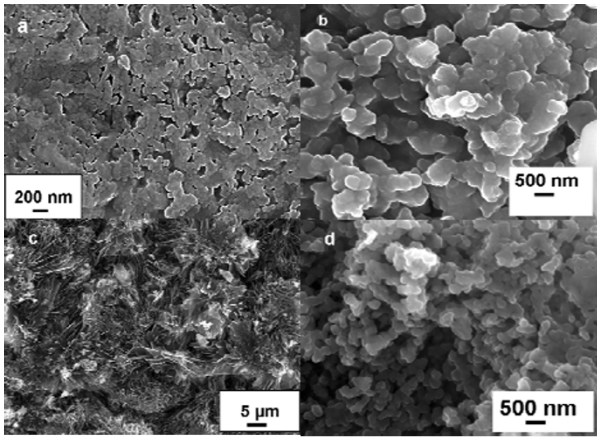

Fig. 2 Gradual development of film microstructure as a function of the number of dipping times: (a) 2, (b) 20, (c) 30 and (d) 60.

The enlarged view of a typical single flower is shown in FE-SEM photomicrograph of Fig. 3(a). This high-magnification photomicrograph proves beyond doubt that there is a definite architectural arrangement of the platelets which gives it a flower-like appearance. Further, FE-SEM photomicrograph of Fig. 3(b) provides evidence that the typical edge thickness of the platelets could vary typically in the range of 30–80 nm.

The detailed view of the central region of such a typical single flower is explored at very high magnification in Fig. 3(c). This FE-SEM photomicrograph establishes the evidence that the center of such a single flower contains dense microstructure of an array of rather straight platelets which emanate nearly from the same region at/in the vicinity of the center, but all of them have corroborative spatial orientation such that a flower petal like arrangement has indeed emerged. The typical length of such straight arrays is about 5–10 μm.

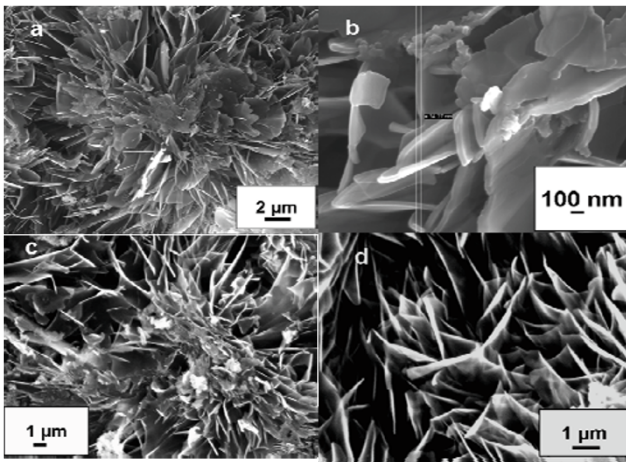

Fig. 3 FE-SEM views of a typical single micro/nano flower structure: (a) architectural arrangement of the platelets; (b) typical edge thickness of the platelets; (c) detailed view of the center; and (d) detailed view of the edges.

Further, it is interesting to note that while the platelets are relatively straighter at the center region, at the edges the platelets are relatively curled (Fig. 3(d)).

The typical TEM view of this flower structure reveals an agglomerated family of nano platelets (Fig. 4). The corresponding lower magnification view is given in Fig. 4(a). The nano size of the platelets becomes more evident at the higher-magnification view (Fig. 4(b)).

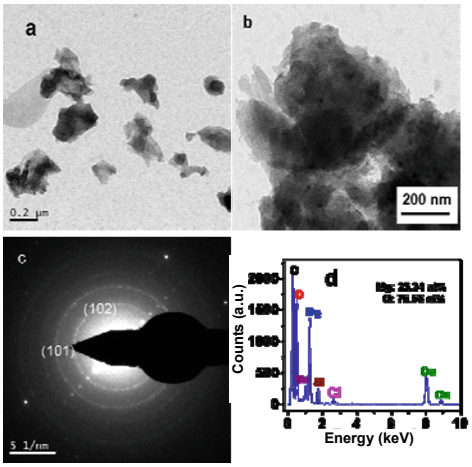

Fig. 4 TEM views of $Mg(OH)_2$ micro/nano flower structure at (a) lower and (b) higher magnifications; (c) corresponding SAED pattern; and (d) typical EDX data.

The data about the corresponding selected area electron diffraction (SAED) patterns are presented in Fig. 4(c). These data show the distinct presence of diffraction circles corresponding to the (101) and (102) peaks. The corresponding estimated values of inter planar spacing (d values) are 2.5 Å and 1.8 Å, respectively. It is worth mentioning that these data match with those obtained from the XRD data [22].

The typical EDX data obtained during TEM study are displayed in Fig. 4(d). These data give 23.34 at% Mg compared well with the reported data [22], and 76.65 at% oxygen. It is suggested further that, the excess oxygen (i.e., 25 at%) possibly comes from SLS glass substrates [22].

To provide a comparative picture of the situation that would occur in absence of SLS glass substrates, FE-SEM photomicrograohs of the chemically synthesized $Mg(OH)_2$ powders obtained after 2, 20, 30 and 60 dippings are shown in Figs. 5(a)–5(d), respectively. In all these photomicrographs, the insets show the typical low-magnification views of the powder aggregates in correspondence. It is evident from these photomicrographs that in absence of SLS glass substrates, the chemically synthesized $Mg(OH)_2$ powders do not have any preferred orientation. However, even at relatively lower number of dipping times, e.g., 20 dippings, the powder particles appear to be arranged in a layered fashion (Fig. 5(b)).

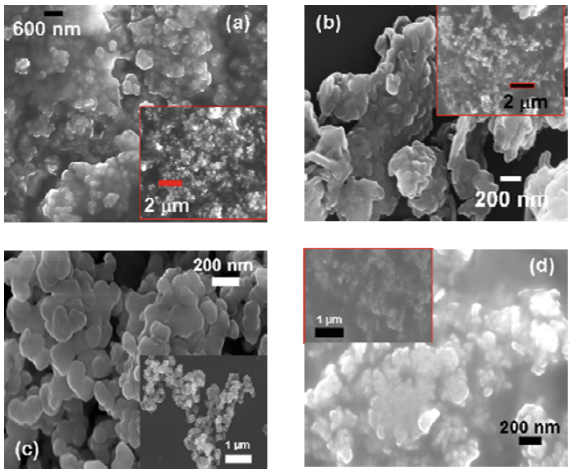

Fig. 5 High-magnification FE-SEM photomicrographs showing the development of microstructure in the chemically synthesized $Mg(OH)_2$ powders as a function of the number of dipping times: (a) 2, (b) 20, (c) 30 and (d) 60. The insets represent the corresponding photomicrographs of the powder agglomerates taken at much lower magnifications.

The localized layered arrangements of the chemically synthesized $Mg(OH)_2$ powders appear to be the most dense in the photomicrograph of the powders

obtained after 30 dippings (Fig. 5(c)). However, the chemically synthesized $Mg(OH)_2$ powders do not appear to reveal any micro/nano flower structure or any specific preferential orientation. At higher number of dipping times, e.g., 60 dippings, the packing density of the powders appears to be locally decreased (Fig. 5(d)). It is also noted that the fine nanocrystallites agglomerate to relatively larger sizes as shown in Figs. 5(a)–5(c).

Therefore, on the basis of the present experimental results, we propose a mechanism for the formation of flower-like surface morphology in the chemically deposited $Mg(OH)_2$ thin films. At the initial stage of dipping, e.g., just 2 dippings, a seed-layer growth of $Mg(OH)_2$ nanoparticles with porous structure has happened (Fig. 2(a)). Support to this conjecture also comes from Fig. 5(a). SLS glass substrates have facilitated their growth in a locally constrained manner.

At a relatively higher number of dipping times, e.g., 20 dippings, a layered platelet structure formation occurs (Fig. 2(b)). The support to this suggestion stems from the photomicrograph presented in Fig. 5(b) as well, which also reveals a partially layered structural growth pattern. The reason for this observation is that in $Mg(OH)_2$, Mg^{2+} bonds to OH^- and then forms a plate-like microstructure [27]. The successive Mg^{2+} ion layers and OH^- ion layers are then stacked one upon another on the existing nuclei which act as the growth centers.

It is suggested that the existence of the nano-sized $Mg(OH)_2$ seed-layer can effectively lower the nucleation energy barrier. This process can then lead to a heterogeneous nucleation stage conducive for most corroborative localized crystal growth [28] at an optimum number of dipping times, e.g., 30 dippings. When this scenario prevails, some of the nuclei may coalesce to form the platelet structures (Fig. 2(c)). Based on the FE-SEM photomicrographic evidence of Fig. 5(c), it is also proposed that depending on the number of dipping times, the structure of individual platelets can be reasonably dense.

Therefore, it is imagined that during the growth process on the pre-existing crystal seeds, the aggregated nano platelets of $Mg(OH)_2$ are self-assembled into a flower-like microstructure. The spatial orientation of such a self-assembly will be governed by the boundary condition that such growth process will decrease the local surface energy through the reduction of the exposed area. A similar mechanism was proposed to explain the formation of ZnO nano flowers on Si substrate [29]. Further research work will be necessary to validate this conjecture.

4 Conclusions

The present work identified for the first time ever the condition that favors the growth of $Mg(OH)_2$ micro/nano flowers in thin films formed on commercially available SLS glass substrates at room temperature. The process involved simple chemical deposition of the thin films by a green and inexpensive alternate dipping technique. The physical structure and microstructure of the chemically deposited films as well as the powders chemically synthesized under identical conditions but without SLS glass substrates were analyzed by XRD, FE-SEM and other techniques. The results obtained in the present work confirmed the formation of nanocrystallites. Based on the XRD, SEM, FE-SEM, TEM and EDX data, it was suggested that the oriented self-assembly of nano platelets have led to the formation of $Mg(OH)_2$ micro/nano flowers in the present thin films. It is proposed further that the decrease in local surface energy through the reduction of exposed area was the driving force behind the formation of $Mg(OH)_2$ micro/nano flowers.

Acknowledgements

The authors acknowledge the kind permission of the director of CSIR-CGCRI to publish this paper. The infrastructural supports received from the XRD and electron microscopy sections of CSIR-CGCRI are highly appreciated. The authors are also thankful to CSIR (Project No. NWP 0027) for financial support.

References

[1] Guo XX, Zhang FZ, Evans DG, *et al.* Layered double hydroxide films: Synthesis, properties and applications. *Chem Commun* 2010, **46**: 5197–5210.

[2] Chakraborty M, Dasgupta S, Sengupta S, *et al.* Layered double hydroxides based ceramic nanocapsules as reservoir and carrier of functional anions. *Trans Ind Ceram Soc* 2010, **69**: 153–163.

[3] Lei XD, Lü Z, Guo XX, *et al.* MgAl-layered double hydroxide films on muscovite mica: Epitaxial growth and catalytic activity in acetone self-condensation. *Ind Eng Chem Res* 2012, **51**: 1275–1280.

[4] Lin C-F, Tsai P-H, Lin Z-Y, *et al.* Solution-processed Li–Al layered-double-hydroxide platelet structures for high efficiency InGaN light emitting diodes. *Opt Express* 2012, **20**: A669–A677.

[5] Huang C-H, Jan Y-L, Lee W-C, *et al.* Investigation of Mg(O,OH) films prepared by chemical bath deposition as buffer layers for $Cu(In,Ga)Se_2$ solar cells. *J Electrochem Soc* 2011, **158**: H879–H888.

[6] Yum J-H, Nakade S, Kim D-Y, *et al.* Improved performance in dye-sensitized solar cells employing TiO_2 photoelectrodes coated with metal hydroxides. *J Phys Chem B* 2006, **110**: 3215–3219.

[7] Zou GL, Liu R, Chen WX. Highly textural lamellar mesostructured magnesium hydroxide via a cathodic electrodeposition process. *Mater Lett* 2007, **61**: 1990–1993.

[8] Zou GL, Chen WX, Liu R, *et al.* Morphology-tunable synthesis and characterizations of $Mg(OH)_2$ films via a cathodic electrochemical process. *Mater Chem Phys* 2008, **107**: 85–90.

[9] Zhu YY, Zhao Q, Zhang Y-H, *et al.* Hydrothermal synthesis of protective coating on magnesium alloy using de-ionized water. *Surf Coat Technol* 2012, **206**: 2961–2966.

[10] Wang PP, Li CH, Gong HY, *et al.* Morphology control and growth mechanism of magnesium hydroxide nanoparticles via a simple wet precipitation method. *Ceram Int* 2011, **37**: 3365–3370.

[11] An DM, Ding XF, Wang ZC, *et al.* Synthesis of ordered arrays of magnesium hydroxide nanoparticles via a simple method. *Colloids Surf A* 2010, **356**: 28–31.

[12] Ding P, Li ZZ, Wang Q, *et al.* In situ growth of layered double hydroxide films under dynamics processes: Influence of metal cations. *Mater Lett* 2012, **77**: 1–3.

[13] Jin DL, Gu XY, Yu XJ, *et al.* Hydrothermal synthesis and characterization of hexagonal $Mg(OH)_2$ nano-flake as a flame retardant. *Mater Chem Phys* 2008, **112**: 962–965.

[14] Wang GZ, Zhang L, Dai HX, *et al.* P123-assisted hydrothermal synthesis and characterization of rectangular parallelepiped and hexagonal prism single-crystalline MgO with three-dimensional wormholelike mesopores. *Inorg Chem* 2008, **47**: 4015–4022.

[15] Li Y, Sui M, Ding Y, *et al.* Preparation of $Mg(OH)_2$ nanorods. *Adv Mater* 2000, **12**: 818–821.

[16] Dhaouadi H, Chaabane H, Touati F. $Mg(OH)_2$ nanorods synthesized by a facile hydrothermal method in the presence of CTAB. *Nano-Micro Lett* 2011, **3**: 153–159.

[17] Shah MA, Al-Marzouki FM. A simple and safe method for preparation of $Mg(OH)_2$ nanorods in ambient air. *Int J Nano Dim* 2011, **2**: 111–116.

[18] Yan CL, Xue DF, Zou LJ, *et al.* Preparation of magnesium hydroxide nanoflowers. *J Cryst Growth* 2005, **282**: 448–454.

[19] Wei Y, Yang R, Yu X-Y, *et al.* Stripping voltammetry study of ultra-trace toxic metal ions on highly selectively adsorptive porous magnesium oxide nanoflowers. *Analyst* 2012, **137**: 2183–2191.

[20] Mukhopadhyay AK, Das PS, Dey A, *et al.* Development and characterization of magnesium hydroxide thin films. *J Inst Eng India Ser D* 2012, **93**: 53–57.

[21] Das PS, Dey A, Chaudhuri MR, *et al.* Chemically deposited magnesium hydroxide thin film. *Surf Eng* 2012, **28**: 731–736.

[22] Lv Y, Zhang ZA, Lai YQ, *et al.* Electrodeposition of porous $Mg(OH)_2$ thin films composed of single-crystal nanosheets. *J Electrochem Soc* 2012, **159**: D187–D189.

[23] Matabola KP. The effects of hydrating agents on the hydration of industrial magnesium oxide. Master Dissertation. Pretoria, South Africa: University of South Africa, 2006.

[24] Yu JC, Xu AW, Zhang LZ, *et al.* Synthesis and characterization of porous magnesium hydroxide and oxide nanoplates. *J Phys Chem B* 2004, **108**: 64–70.

[25] Phillips VA, Opperhauser H, Kolbe JL. Relations among particle size, shape, and surface area of $Mg(OH)_2$ and its calcination product. *J Am Ceram Soc* 1978, **61**: 75–81.

[26] Gutowski JR, Richmond A. Wet milling of $Mg(OH)_2$ slurry. European Patent CA 2300947, 1998.

[27] Turek M, Gnot W. Precipitation of magnesium hydroxide from brine. *Ind Eng Chem Res* 1995, **34**: 244–250.

[28] Sun HK, Luo M, Weng WJ, *et al.* Position and density control in hydrothermal growth of ZnO nanorod arrays through pre-formed micro/ nanodots. *Nanotechnology* 2008, **19**: 395602.

[29] Li Q, Sun H, Luo M, *et al.* Room temperature synthesis of ZnO nanoflowers on Si substrate via seed-layer assisted solution route. *J Alloys Compd* 2010, **503**: 514–518.